Tribology International 180 (2023) 108264

Contents lists available at ScienceDirect

Tribology International

journal homepage: www.elsevier.com/locate/triboint

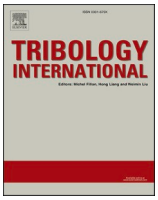

Multifunctional steel surface through the treatment with graphene and h-BN

María J.G. Guimarey [a,b,*], Chirag R. Ratwani [b], Kaiyu Xie [c], Mehran Koohgilani [b], Mark Hadfield [b], Ali Reza Kamali [c,d], Amor M. Abdelkader [b]

[a] Laboratory of Thermophysical and Tribological Properties, Nafomat Group, Department of Applied Physics, Faculty of Physics and iMATUS, University of Santiago de Compostela, 15782 Santiago de Compostela, Spain
[b] Department of Design and Engineering, Faculty of Science & Technology, Bournemouth University, Poole, Dorset BH12 5BB, United Kingdom
[c] Energy and Environmental Materials Research Centre (E2MC), School of Metallurgy, Northeastern University, Shenyang 110819, China
[d] Department of Materials Science and Metallurgy, University of Cambridge, Cambridge CB3 0FS, United Kingdom

ARTICLE INFO

Keywords:
Graphene nanoplatelets
Hexagonal boron nitride
Nano-treatment surface
Friction

ABSTRACT

The search for improved surface properties of engineering alloys is always a matter of interest. Herein, we introduce a surface treatment based on depositing a non-continuous layer of two-dimensional (2D) nanomaterials via a simple and scalable method. 2D nanosheets of hexagonal boron nitride (h-BN) and graphene nanoplatelets (GNP) were sprayed on mild steel, followed by mild heat treatment. The nanosheets are strongly attached to the surfaces and even diffused to submicron under the surface, as proved by various analytical techniques. The mechanical, tribological and corrosion evaluations show significant simultaneous enhancement in a set of surface properties. From the friction tests with sliding steel-steel tribo-pairs under dry conditions, the graphene treatment decreases the friction coefficient and wear area by 21% and 31%, respectively. Interestingly, it is revealed that under dry and lubricated conditions, graphene-doped h-BN exhibits outstanding anti-wear properties synergistically compared to stand-alone 2D materials. The possible wear mechanism is investigated and found to be based on the formation of a tribofilm.

1. Introduction

In 2017 almost a quarter (about 23%) of the total worldwide energy consumption came from tribological contacts. In economic terms, the total annual losses caused by tribological contacts are estimated to be 2536,000 million euros, being 73% due to friction and 27% due to wear [1]. Therefore, mechanical failures related to friction and wear enhancement remain among the biggest challenges for mechanical transmissions in motion [2]. Most traditional methods of reducing friction and wear involve the use of solid and/or liquid lubricants. Although optimum tribological performance has been achieved using formulated lubricants, the search for a more environmentally efficient lubricant continues. Surface hardening is an effective process used to improve the wear resistance of steel surfaces without affecting their internal toughness, ideal for components such as cams and gears, which withstand high impacts [3]. Consequently, finding a solid lubricant that can be used as a coating on steel to increase its surface hardness may be a promising solution to the industry's tribological challenge today.

In addition, most moving mechanical transmissions are made of metallic materials. Specifically, mild steel is one of the most commonly used steel grades in many engineering applications due to its attractive properties compared to its relatively low cost [4]. Due to its exposure to the environment, the metallic materials are at risk of corrosion without forming a protective surface layer, which leads to material degradation, entailing high maintenance costs for the industry [5]. Using anti-corrosion alloys and coatings is considered one of the most effective methods to address the metal corrosion in moving parts [6]. However, although the use of corrosion-resistant alloys has dramatically mitigated metallic materials' corrosion problem, it is an expensive approach since most corrosion-resistant alloys contain high amounts of chromium and nickel. In addition, most of these costly alloys have limited durability under aggressive loading conditions [7]. Therefore, different surface coating methods have started to be widely used in the industry, including resurfacing welding [8], laser cladding [9,10], inductive

* Corresponding author at: Laboratory of Thermophysical and Tribological Properties, Nafomat Group, Department of Applied Physics, Faculty of Physics and iMATUS, University of Santiago de Compostela, 15782 Santiago de Compostela, Spain.
E-mail addresses: mariajesus.guimarey@usc.es, mgarciaguimarey@bournemouth.ac.uk (M.J.G. Guimarey).

https://doi.org/10.1016/j.triboint.2023.108264
Received 4 August 2022; Received in revised form 28 December 2022; Accepted 12 January 2023
Available online 13 January 2023

cladding [11] and thermal spraying [12]. However, they all have a relatively high processing cost and operational inconvenience. The spray method is a simple technique in which a gas stream accelerates the powder solution at high speed. Due to its high throughput deposition on large surface areas, this versatile technique generates low waste. It can be used on different surfaces regardless of their morphology, allowing the use of a wide range of fluids with other rheological properties [13]. Hence, the spray method has a low processing cost, high working efficiency and operational convenience making it ideal for processing nanomaterial coatings.

Frequently, heat treatments are used to increase the mechanical and wear resistance of the mild steel. Carburising and nitriding are the most used surface hardening processes, introducing carbon or nitrogen atoms to the surface of low-carbon steels at temperatures generally between 860 °C and 940 °C [14]. Despite their proven ability to improve the surface properties, the high operation temperature might alert the other bulk properties of the materials, in addition to the significant increase in the cost. Another famous heat treatment process is tempering, which reduces internal stresses and increases steel toughness and durability [15]. An inert atmosphere is usually used during the heat treatment to prevent oxidation and decarburisation in steel. Thus, it is useful to develop a surface treatment process that avoids overlapping with the traditional retreatment process but rather provides oxidation resistance during heating above the eutectoid point. Heat treatment of nano-coatings could address this challenge due to the achievement of enhanced adhesion with the substrate caused by the formation of metallurgical bonding provided by the diffusion coatings [16].

Finally, the proper selection of spray coating materials is crucial to obtain a protective layer on metal surfaces capable of improving their tribological, mechanical and corrosion properties. In recent years, great attention has been paid on using 2D materials as metal-reinforcing coatings. Among the two-dimensional (2D) materials, graphene and hexagonal boron nitride (h-BN) stand out as protective coatings due to their layered structure and excellent chemical resistance, barrier properties, impermeability, and thermal stability [17]. In addition to these unique properties, graphene possesses remarkable chemical inertness, which, together with its excellent impermeability to gases and liquids, gives graphene coatings on metals excellent corrosion resistance [7]. Nonetheless, graphene's ability to protect metal surfaces may be affected by galvanic corrosion problems. In this aspect, it has been confirmed that the good electrical insulation of h-BN prevents galvanic corrosion and makes its anti-corrosion capacity superior to that of graphene [17], so h-BN is a better alternative for anti-corrosive coatings because of its electrical insulation nature. However, compared to the widespread concern that graphene has caused in the anti-corrosion field, there are few research reports on the long-term corrosion resistance of h-BN to metals.

Therefore, developing a reliable and easy-to-use method to obtain multifunctional surfaces (higher hardness, lower friction, increased wear and corrosion resistance) would be a major breakthrough in any industrial application in terms of energy and cost savings. The current work investigates the tribological, mechanical and corrosion performance of various 2D nanomaterials as potential steel surface reinforcing materials. Thus, GNP, h-BN and h-BN/GNP nanoadditives are spread on the mild steel substrate using a simple spray method combined with subsequent heat treatment at low temperatures. The concept presented in the current work is a promising alternative to high-temperature hardening, with even more enhanced tribological performance, corrosion resistance, and excellent tolerance to high-temperature dry oxidation.

2. Experimental procedure

2.1. Samples preparation

GNP (average lateral size 3 μm) was obtained by the cathodic electrochemical exfoliation as described elsewhere [18]. h-BN (particle size of 18 μm) was obtained by the mechanochemical intercalation process using metallic lithium as the intercalating agent as described in our previous work [19]. The additives, GNP, h-BN and h-BN/GNP were suspended by sonication (24 h) in a water/ethanol solution (1:1) with a weight concentration of 1 mg/mL. Bright drawn mild steel samples grade EN3B of 2.5 × 2.5 cm^2 area was used as the model substrate material, which was previously polished to a mirror finish (Ra < 70 nm). The chemical composition of the EN3B mild steel samples used as substrates for friction, hardness and corrosion tests is listed in Table S1 (Supplementary material) [20]. The spray method spread solutions containing nano-additives on the highly polished steel substrates. The process is based on incorporating 2D nanomaterials (h-BN, GNP and the hybrid h-BN/GNP) into the surface layer of the metal substrate using a Laval nozzle sprayer connected to an air compressor. The nano-treated surfaces were subjected to mild heat treatment over a wide range of temperatures (200, 300 and 400 °C) and holding times (2, 4 and 6 h) to study the effect of heat treatment on micro-hardness properties. Heat treatments were carried out in a tube furnace under a modified Argon atmosphere to avoid the presence of oxygen and prevent oxidation. All samples were heated at a rate of 5 °C/min and cooled in the furnace.

Table 1
Ball-on-plate test parameters.

Parameters	Value
Load (F_n)	5 N
Maximum Hertzian contact pressure	1.2 GPa
Sliding speed	0.1 m s^{-1}
Sliding distance (S_n)	100 m
Amplitude	10 mm
Acquisition rate	100 Hz

2.2. Surface treatment characterisation

To analyse the composition of nano-treated surfaces, fully confocal Horiba XploRATM was used for Raman mapping with a 532 nm laser. The measurement conditions were optimised to avoid fluorescence and obtain a higher signal-to-noise ratio. All mapping was done at the centre of the steel sample, and 8000 points were collected, 20 each in X, Y, and Z directions using an objective lens of 50x. All data were processed with LabSpec 6 software. A field emission scanning electron microscope (SEM, Zeiss Ultra Plus) equipped with a dispersive energy X-ray (EDS) detector and a transmission electron microscope (TEM, Tecnai F20 operating voltage at 200 kV) were employed for morphological characterisations. Surface analysis was conducted by X-ray photoelectron spectroscopy (XPS, ESCALAB250, Thermo Fisher Scientific).

Finally, 3D optical profilometry was used to determine the roughness surface, Ra, of both unnano-treated and treated samples according to ISO4287 (Gaussian filter with a cut-off wavelength of 0.08 mm).

2.3. Vickers hardness tests

The hardness of untreated and nano-treated mild steel samples was measured with a Buehler hardness tester using the Vickers hardness method. In the Vickers hardness test, a load is applied gently, without impact, by forcing a diamond indenter into the test specimen. The Vickers diamond produces a square-based pyramidal shape, and the two diagonals of the impression are measured with an optical microscope and averaged. Tests were performed according to British Standard BS 427 under the major load of 50 kgf with a loading speed and time of 50 μm s^{-1} and 10 s, respectively, using a Vickers diamond indenter. The arithmetic mean of at least five measurements was given as the average hardness value of the samples.

Table 2
Properties of formulated 5W-30 engine oil.

Physicochemical properties	Value
VI	163.3
$\rho_{298\ K}$ / km m^{-3}	848.6
$\nu_{303\ K}$ / $mm^2\ s^{-1}$	112.74
$\nu_{373\ K}$ / $mm^2\ s^{-1}$	11.83

2.4. Tribological tests

Tribological studies of untreated and nano-treated mild steel flat substrates against chrome steel balls were performed in the air (40% RH) at room temperature using a CSM tribometer with a ball-on-plate contact geometry in a linear mode. The acquisition parameters are gathered in Table 1. Four different mild steel substrates were studied: untreated and the three nano-treated with 200 layers of GNP, h-BN and the hybrid h-BN+GNP, respectively. The static partners were the 100Cr6 steel balls supplier by PCS Instrument with 6 mm of diameter, 803 HV of hardness, 210 GPa of Young's modulus, 0.29 of Poisson's ratio and 32 nm of average surface roughness. All friction sliding tests were repeated at least three times, and the mean values with its respective standard deviation were calculated.

Sliding friction tests were performed for untreated and nano-treated steel substrates, first under dry lubrication conditions and then using a fully formulated commercial oil, 5 W-30, widely used in diesel engines. This engine oil was previously characterised [21], and its main physicochemical properties are listed in Table 2. The objective was to compare the tribological performance of the nano-treated surfaces under dry and lubricated conditions.

2.5. Surface wear analysis

Images, cross-sectional profiles and dimensions (wear track width, WTW, area and volume) of wear scars produced on the substrates by the friction tests were evaluated with a Sensofar S Neox 3D optical profilometer, working in confocal mode using a 10 × objective and the SensoMAP software, integrated with the profiler, which provides fast and accurate analysis of surface geometry. Wear dimensions were evaluated in three different zones for each worn track to obtain average values. In addition, the roughness (Ra) of the abraded substrates was determined according to ISO 4287 (Gaussian filter with a cut-off wavelength of 0.08 mm). Roughness values are averages of at least three measurements. In order to identify possible tribological mechanisms produced by the presence of nanoadditives on the abraded surfaces, a WITec alpha300R+ confocal Raman microscope was used at 532 nm.

2.6. Corrosion study

The corrosion activity of different nano-treated mild steel surfaces was evaluated. Bare and nano-sprayed samples were heat-treated at 300 °C for 4 h under an inert atmosphere and then exposed to air at room temperature with a relative humidity of 40–60% for six months. The steel samples were previously cleaned with hexane in an ultrasound bath and dried with hot air. At the end of the corrosion test, the substrate surfaces were analysed by two complementary methods. Initially, a simple visual inspection of the surface of the substrates was made, and then scanning electron microscopy (SEM) was employed to determine the presence of corrosion.

To further understand the anti-corrosion properties of the nano-treated surfaces, Electrochemical Impedance Spectroscopy (EIS) and potentiodynamic polarisation measurements were performed in a three-electrode cell using Iviumstat Electrochemical Interface in simulated seawater media (3.5% NaCl) at room temperature for all the samples at their respective OCP values. The bare/nano-treated mild steel substrate formed the working electrode, whereas a silver/silver chloride (Ag/AgCl) electrode and a platinum electrode served as the reference and counter electrodes, respectively. The designed electrochemical cell keeps a surface area of 3.14 cm^2 of the samples exposed. All samples were kept in solution for 60 min to reach the open-circuit potential. EIS measurements were performed in the frequency range of 1 MHz to 0.01 Hz with the sinusoidal signal amplitude of 5 mV. IviumSoft software and OriginPro were used for data acquisition and analysis. The corrosion potential (E_{corr}), corrosion current density (I_{corr}) and corrosion rate (C_{rate}) were determined using the Tafel extrapolation method. Polarisation tests were carried out from a cathodic potential of − 0.25 V to an anodic potential of 0.25 V with respect to OCP at a scan rate of 0.5 mV s^{-1}.

3. Results and discussion

3.1. Surface treatment characterisation

The first evidence of modifying the steel with the 2D materials can be obtained from the EDX analysis of the samples' surfaces. As can be seen from Fig. 1, nitrogen is homogeneously distributed on the steel after spraying h-BN. The Raman mapping (Fig. S1) also proves that the steel surface contains h-BN and/or graphene. The typical h-BN peaks at 1367 cm^{-1} [22] could be detected across the sample's surface treated with individual or heterogeneous 2D materials. The typical 2D peak of GNP at around 2721 cm^{-1} [23] could also be detected when GNP is used alone or hybridised with h-BN. The XPS survey scan could also detect nitrogen (Fig. 2), further proving the existence of h-BN. A high-resolution scan of the Fe 2p spectrum showed, in addition to the Fe^{3+} peaks at 710.05 eV and 723.65 eV, two satellite peaks at 717.66 eV and 732.72 eV could be detected, indicating the formation of the Fe-N bond [24,25]. The small Peak at ~706 could also be assigned to the Fe_xN.

Although the high-resolution scan of the N1s spectra could be recorded for the steel samples treated with h-BN, its intensity did not clearly distinguish the type of the N bonding. However, the peak at

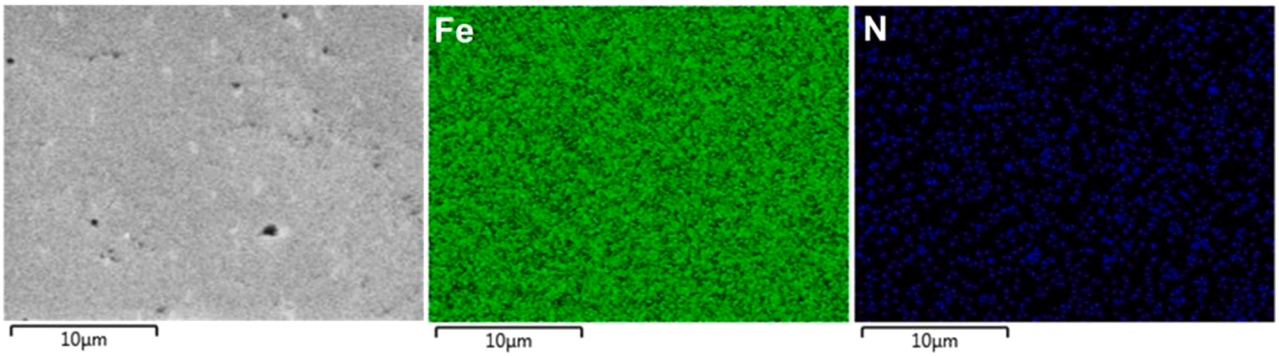

Fig. 1. EDX analysis of the h-BN-treated steel surface.

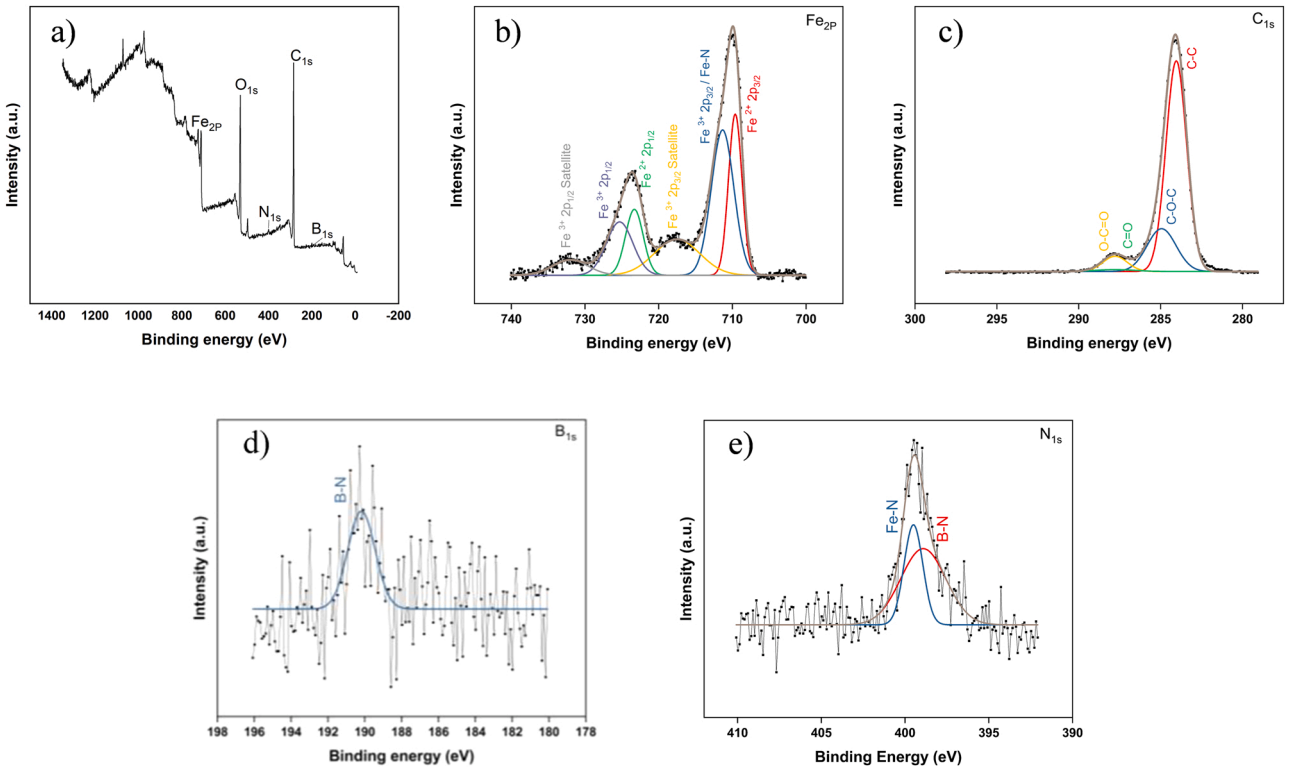

Fig. 2. a) XPS survey scan data, b) Fe2p spectrum, c) C1s spectrum, d) B1s spectrum, and e) N1s spectrum of h-BN surface treatment steel.

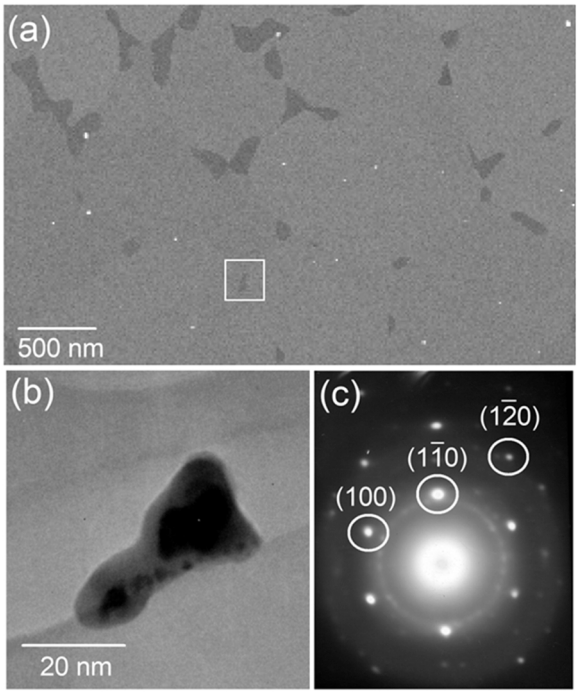

Fig. 3. (a) TEM micrograph taken from the cross-section of h-BN treated steel exhibiting the presence of nanoparticles. (b) High magnification micrograph of a nanoparticle, and (c) the diffraction pattern recorded on the nanoparticle showing diffraction spots corresponding to various crystalline planes of the h-BN.

~399 indicates bonding between nitrogen and iron. Both $Fe2p_{3/2}$ and N1s spectra suggest that h-BN is not only physically attached to the steel surface but rather chemically interacted with the substrate.

To understand the extent of the nanoparticle's interaction with the steel substrate, the structure of transverse thin sections of the samples treated with various nanosheets was studied. Fig. 3a shows a typical TEM micrograph recorded on the sample, in which the presence of nanoparticles with sizes of around 20 nm within a depth of around a few micrometres from the surface is evident. Fig. 3b exhibits a higher magnification micrograph taken from a nanoparticle, and Fig. 3c shows the diffraction pattern recorded on the nanoparticle, from which the presence of a typical hexagon of the h-BN with a brighter first ring can be observed, suggesting a typical monolayer flake. This finding indicates that some of the nanosheets could still diffuse within the steel substrate without breaking into the atomic or molecular level. Indeed, these subsurface nanosheets are responsible for alerting the surface properties, as will be discussed later in this article. It is worth noting here that detecting graphene was more difficult than h-BN due to the overlapping between the graphene flakes and the carbon-containing phases in the steel. The SEM images taken for the cross-section proved that h-BN diffused within the steel substrate with a depth of 20–50 μm (Fig. S2c). On the other hand, GNP formed a distinguished layer on the steel surface. Some cracks and gaps between the GNP and the substrate steel can be observed.

Roughness surface was measured for both bare and treated samples. A decrease in the roughness can be observed when the nanoadditives are deposited on the steel surface. The highest roughness reduction, around 86%, was produced with the h-BN/GNP treatment, from 66 nm Ra corresponding to the bare sample to 9 nm. GNP and h-BN-based treatments achieved a roughness surface of 16 and 13 nm, respectively. The smoother surface is due to the uniform and quick spreading of the droplets nanoadditives, avoiding over-wetting of the surface, which can lead to droplets on the surface of the sprayed film and the formation of rougher films [26]. The enhanced performance of the hybrid treatment can be understood by comparing the surface morphologies of different samples. The synergy between the h-BN nanoflakes diffused into the substrate and the surface GNP provided a double smoothing effect on the steel surface.

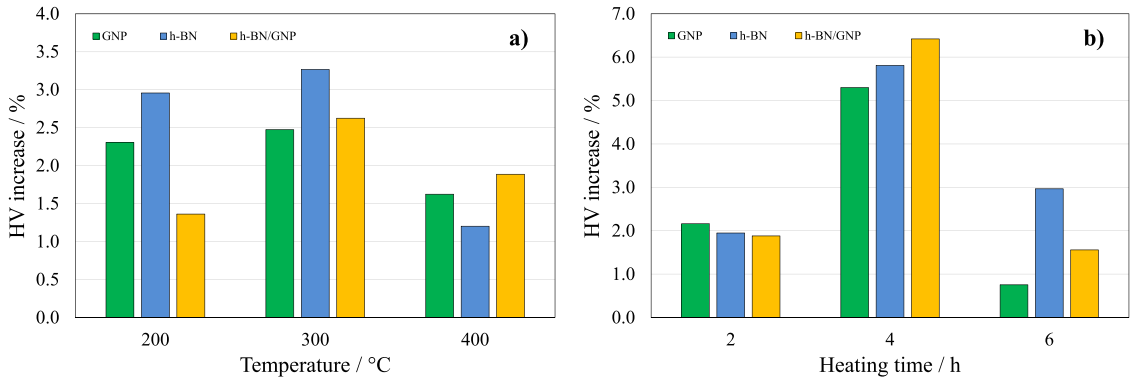

Fig. 4. Vickers hardness increase of steel substrates treated with 200 spray rounds of different 2D nanomaterials at different a) temperatures and b) heating times.

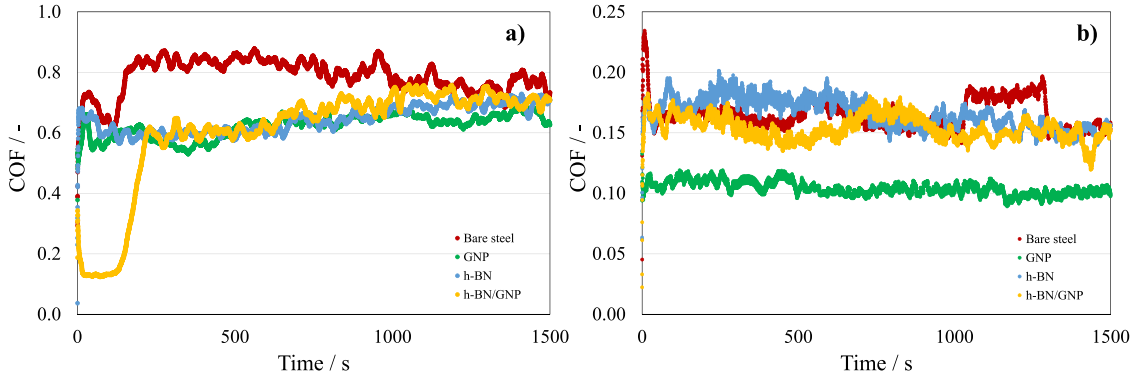

Fig. 5. The evolution of the coefficient of friction (COF) of surface untreated and treatment with nanoadditives: a) dry and b) lubricated conditions.

3.2. Vickers hardness

Different post-heating temperatures (200, 300 and 400 °C) and heating exposure times (2, 4 and 6 h) were tested to find the optimum heating conditions for the highest hardness performance. The first hardness test was performed on the bare steel substrate and on steel substrates treated with 200 spray rounds of each nano-additive (GNP, h-BN and h-BN/GNP hybrid). The variation of the Vickers hardness of the treated samples compared to the bare sample was plotted in Fig. 4a. The hardness results show a greater improvement in this property for substrates treated with a post-heat treatment at 300 °C, with increases of 2.5%, 3.3% and 2.6% being achieved for the 200 spray rounds of GNP, h-BN and h-BN/GNP compared to the bare steel substrate, respectively. Increasing the treatment temperature from 200°C to 300°C results in a clear increase in the hardness of all samples, with a more pronounced effect for the hybrid nanoparticle treatment. On the other hand, they were decreasing the hardness of all the samples at higher treatment temperatures suggesting some softening in the materials.

One challenge of using nanoparticles for nitriding or carbonising steel is the slow diffusion into the substrate. In the current case, where there is some evidence that GNP and h-BN are diffusing in the form of tiny flakes not only in their atomic form, the diffusion is expected to be slow. To understand the effect of the treatment time on the nanoparticle's diffusion and interaction with the substrate, the hardness of various types of surface nano-treatment at 300 °C was measured at different heating times: 2, 4 and 6 h. Fig. 4b clearly shows that the highest increase in hardness of the steel substrates takes place for the nano-treatments with a heating time of 4 h, achieving an increase in hardness of around 5.3%, 5.8% and 6.4% for the steel treated with GNP, h-BN and h-BN/GNP when compared to the bare steel substrate, respectively. We believe that the decrease of hardness at prolonged treatment time is probably due to the tempering effect and the removal of the surface residual stresses that contributed to the hardness. From the Vickers hardness tests, it has been concluded that the optimum heating conditions in terms of hardness increase are 300 °C for 4 h. Therefore, these were the nano-treatment parameters selected to prepare the steel surfaces used in the tribological tests.

3.3. Tribological performance

Sliding friction tests were performed on bare and treated substrates with 200 spray rounds of each nanomaterial (GNP, h-BN and h-BN/GNP) and heated at 300 °C for 4 h first in dry conditions and then using a commercial oil as a lubricant. Fig. 5 shows the evolution of the coefficient of friction (COF) during the total duration of ball-on-plate friction tests for untreated and nano-treated mild steel surfaces in dry and wet conditions. Under dry conditions (Fig. 5a), the COF for bare steel surface was initially low (~0.4), then increased rapidly with the removal of the surface contaminants and/or a natural oxide layer from the surface, reaching a value of about 0.8. The high COF with relatively large deviation is observed for the non-treated surface. In contrast, the variation of COF is smaller for the nano-treated surfaces, with a stable evolution can be observed for both for the GNP and the h-BN surface treatment. Interestingly, there is a noticeable improvement in the COF of nano-treated surfaces. In the case of the nano-treated hybrid substrate, the COF fluctuated during the first 100 s of the test, showing an initial decrease followed by a gradual increase until it reached a stable value, as is the case of bare steel.

On the other hand, for the lubricated sliding friction tests, as expected, the COF is reduced under the influence of the engine oil. Interestingly, the GNP-treated surface revealed the most considerable anti-friction enhancement, reducing the average COF by 15% with respect to the untreated steel (Fig. 5b). This effect can be attributed to a mechanical action of graphene related to its load-carrying capacity [27]

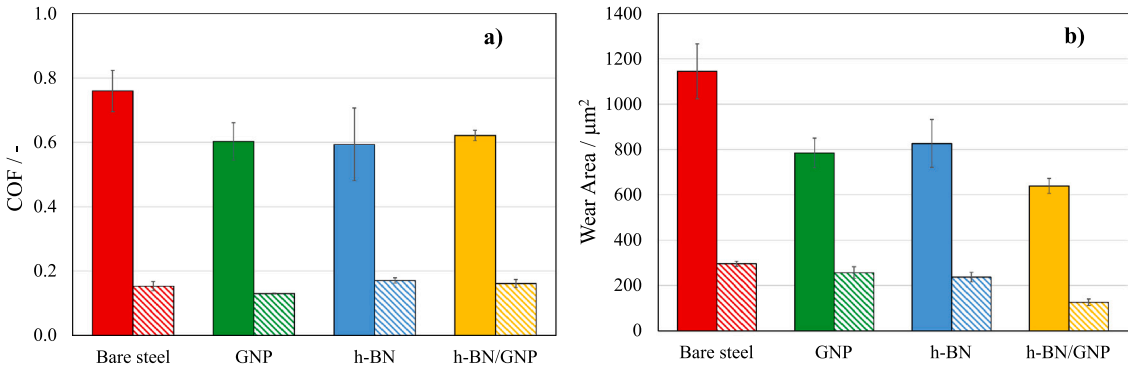

Fig. 6. The influence of surface treatment with nanoadditives on tribological performance: a) coefficients of friction and b) wear cross-sectional area for bare and treated substrates in two different lubrication conditions: dry (filled bar) and lubricated (grated bar).

due to the weak Van der Waals force between the graphene layers in the nanoplatelets and their atomically smooth surface, which favours self-lubrication and interlayer sliding that dampens the contact interfaces [28].

The average COF results comparing the bare and treated substrates in both dry and lubrication conditions are plotted in Fig. 6a. For dry lubrication conditions (colour-filled bars), excellent anti-friction behaviour is revealed for all treated surfaces compared to the bare metal. The best result was obtained for the steel treated with h-BN, reaching a coefficient of friction (COF) reduction of 22% compared with bare steel. This is not the case when an oil (5W-30) is used as a lubricant between the contact surfaces during sliding friction tests. Only the GNP-treated substrate produces a 15% improvement in COF over the bare sample; the h-BN and hybrid treatments do not achieve this anti-friction effect when 5W-30 lubricant is used. This is understandable considering the nature of the steel surface after various treatments. Since GNP mainly coats the surface and smoothes it down almost to the atomic level, it facilitated further sliding when the lubricant was added.

After the friction tests, the wear scars produced on the substrates were optically measured. Fig. 6b shows the worn track's cross-sectional area tested under dry (colour-filled bars) and lubricated conditions (grated bars). Once again, excellent anti-wear performance was revealed for the substrates treated with the nanoadditives. The hybrid nanomaterials treatment shows the best resistance to wear, reaching 44% reduction in the scar area under dry lubrication. The GNP and h-BN nano-treatments reduce the steel substrate's wear area by 31% and 28%, respectively. As in previous works [29], it is observed that the synergy of both nano-additives has the best anti-wear performance. These wear resistance results agree with the improvement in micro-hardness, with the h-BN/GNP surface treatment conferring the greatest hardening (6.4% increase) to the steel substrate.

To better understand the influence of nanoadditives on the wear resistance, the cross-sectional profiles and the optical images of wear tracks were obtained with a 3D optical profiler under dry and lubricated conditions (Fig. S3 and S4). Fig. S3a displays the cross-sectional profiles of worn scars under dry conditions and Fig. S3b under lubricated conditions using 5W-30 engine oil. Clearly, it can be observed that when engine oil is used to lubricate the steel-steel contact, the wear track profiles corresponding to the nanoparticles treated steel have smaller track width and depth and are smoother, especially for the h-BN/GNP. It is important to note that the irregularities in the profiles of the wear tracks disappeared with nanoadditives surface treatment, leaving a smooth and homogenous surface both inside and outside the wear track. Thus, a polishing effect is observed on the wear tracks, as the surface of steel treated with GNP, h-BN, and the hybrid of both show a much smoother profile, while the same wear track profile for uncoated steel shows a high roughness. This effect is much more noticeable for surfaces lubricated with commercial engine oil. Optical images (Fig. S4) reveal a greater homogeneity of the surfaces treated with nanoparticles outside

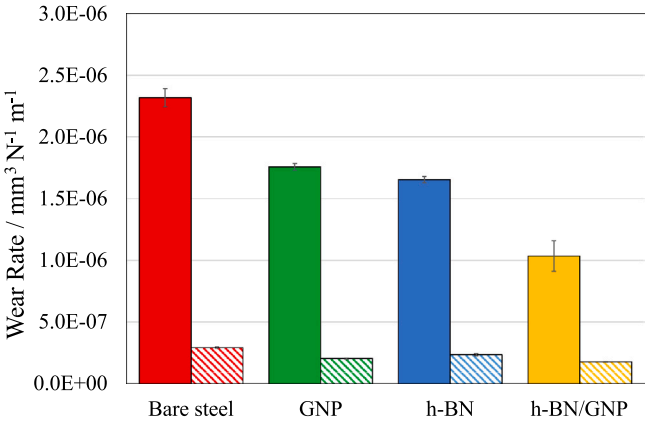

Fig. 7. Specific wear rate from the sliding tests for bare and treated substrates in two different lubrication conditions: dry (filled bar) and lubricated (grated bar).

the worn area (surface blue colour). At the same time, for bare steel, it is observed that the surface has numerous scratches and grooves. The spraying method allows the deposition of the nanomaterials on the surfaces, which, due to their nanometric size, manage to penetrate the existing imperfections on the polished surface and thus reduce its roughness. This phenomenon is more pronounced for the surface treated with h-BN/GNP hybrid. This is believed to be due to the wear mechanism's evolution due to the steel substrate's hardness variation (6.4% increase in hardness when the surfaces were treated with h-BN/GNP) [28].

The specific wear rate was determined from the residual groove volume loss in the mild steel substrates (untreated and treated) and calculated using the following equation [30]:

$$W = \frac{\Delta V}{F_n S_n} \tag{1}$$

where W is the specific wear rate ($mm^3\ N^{-1}\ m^{-1}$), ΔV is the volume loss (mm^3), F_n is the applied load (N), and S_n is the sliding distance (m). The volume loss was measured with SensoMAP software, inputting the level of the unworn surface using the hole perimeter at this level. The software then automatically determines the coordinates of the profile points of the wear surface and calculates the hole volume below this level. F_n and S_n are listed in Table 1. The wear rates calculated for untreated and treated substrates are plotted in Fig. 7. All surface treatments reduce the wear rates compared to the untreated steel, confirming the results observed for the wear area. The reductions in wear rates obtained with the different surface treatments compared to the bare surface have been: 24%, 29% and 55% in dry tests and 30%, 20% and 39% in wet tests for

Table 3
Average surface roughness (Ra) and its standard deviation (σ) for the bare and treated steel.

Substrate	Ra /nm	σ /nm	Ra /nm	σ /nm
	DRY		LUBRICATED	
Bare	170	23.8	55.6	4.11
GNP	146	17.7	41.4	2.27
h-BN	169	24.5	28.7	1.29
h-BN/GNP	165	23.6	35.6	1.11

GNP, h-BN and h-BN/GNP, respectively. The lowest wear rates were observed for the surfaces treated with h-BN/ GNP, which also showed the highest hardness (Fig. 4b) and the lowest friction (Fig. 5a). The bare steel exhibits a specific wear rate of 2.3 10^{-6} mm^3 N^{-1} m^{-1} under 5 N load in dry conditions and this value decreases to 1.0 10^{-6} mm^3 N^{-1} m^{-1} for the h-BN/GNP treated steel. Such high wear rate reductions reflect the effective action of nanoparticles on the tribological properties of the mild steel and provide enormous protection against material loss, thus increasing the service life of the machinery and considerable savings [31].

Finally, the roughness (Ra) of the worn tracks was also measured (Table 3) to analyse the anti-wear ability of the nanomaterials treated steel since the wear mechanism is strongly dependent on the surface roughness [32]. Lower roughness after friction tests was obtained for the surfaces lubricated with 5W-30 engine oil than those without lubricant. Precisely, the Ra value of the bare steel is 170 nm under dry conditions and reduced to 56 nm when lubricant oil is applied (three times lower). Furthermore, for the engine oil lubricated friction tests, it is observed that the roughness decreases by 26%, 48% and 36% for the GNP, h-BN and h-BN/GNP treated surfaces with respect to the bare steel, respectively. As a result, it can be concluded that a polishing effect occurs due to nano-additives [33], as observed in the cross-section profiles of the wear tracks (Fig. S3). Otherwise, under dry lubrication conditions, the roughness decreases slightly with the use of the nanoparticles treated surface. In contrast to the lubricated conditions, the treated steel in dry lubrication conditions has a low influence on roughness, as seen in Fig. S3.

Raman mapping of the h-BN/GNP treated worn surface (Fig. 8) was carried out to identify the role of nanoparticles in wear reduction. The

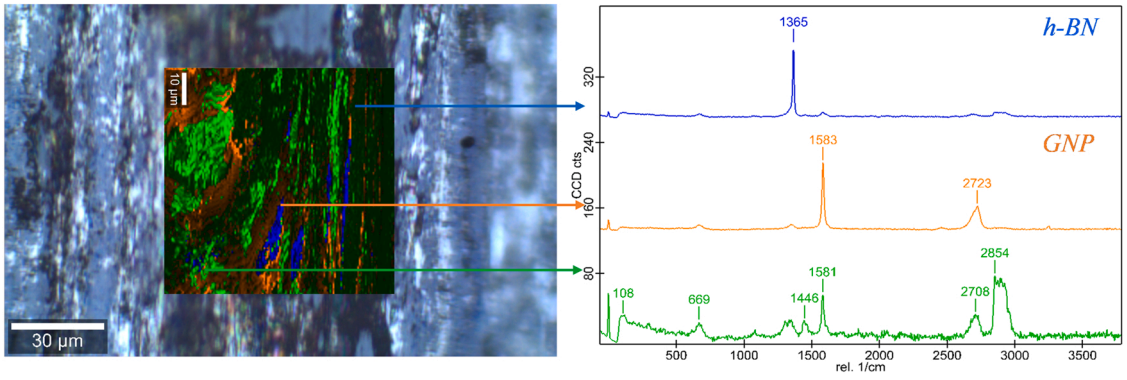

Fig. 8. Elemental mapping and Raman characterization of worn surface obtained with the h-BN/GNP treated steel surface.

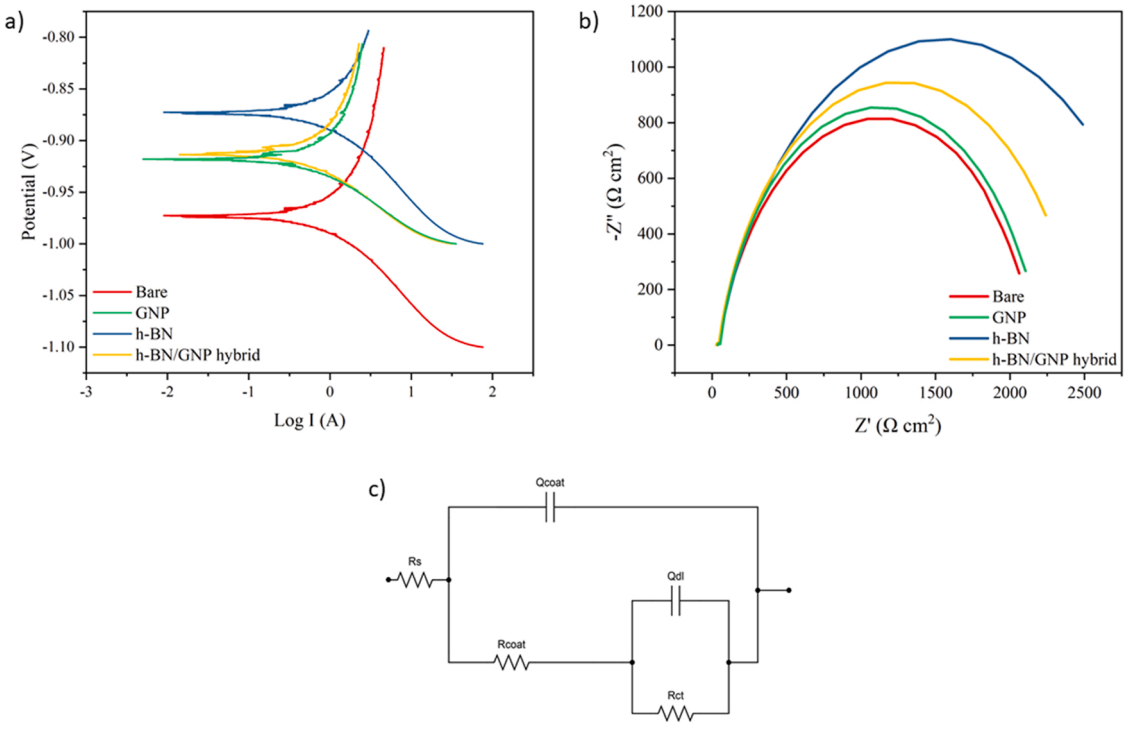

Fig. 9. Electrochemical test results of bare and treated steel in 3.5% NaCl solution: (a) Nyquist plot, (b) Tafel plot, and c) simulated equivalent circuit.

Table 4
Potentiodynamic polarization parameters of bare, GNP-, h-BN-, and h-BN/GNP-treated mild steel specimens.

Sample	E_{corr} / V	I_{corr} / A cm^{-2}	C_{rate} / mm y^{-1}
Bare	-0.989	5.667 10^{-7}	6.676 10^{-3}
GNP	-0.940	5.296 10^{-7}	6.241 10^{-3}
h-BN	-0.931	3.321 10^{-7}	3.913 10^{-3}
h-BN/GNP	-0.930	3.370 10^{-7}	3.971 10^{-3}

Raman mapping of the unworn steel surface (Fig. S1) shows the characteristic peaks of h-BN (1367 cm^{-1}) [34] and GNP (2721 cm^{-1}) [35]. The Raman spectrum inside the wear track (Fig. 8) detects these peaks and confirms the distribution of the nanoadditives in the wear track. Specifically, the relevant areas in blue (h-BN) and in orange (GNP) are clearly visible in the sliding direction along the grooves produced, as shown in Fig. 8. This indicates that tribofilms containing h-BN and GNP were formed on the worn surface during the friction test. Therefore, it can be concluded from the Raman and roughness results that the main tribological mechanism occurring with the hybrid surface treatment is tribofilm formation. Another relevant observation is that the existence of tribofilms of the nanoadditives after the friction tests reveals a good adhesion of the surface treatment on the steel substrate, maintaining the presence of the h-BN/GNP after the contact pressure exerted.

3.4. Corrosion resistance

The surfaces treated with 2D materials show great ability to resist atmospheric degradation. The EIS and potentiodynamic polarisation measurements were performed to compare the corrosion rate of bare mild steel and GNP, h-BN, and h-BN/GNP treated samples in 3.5 wt% NaCl solution. Fig. 9 shows the Nyquist and Tafel plots obtained for all samples, and the corrosion rate was determined from the extrapolation of these curves. The Tafel plot parameters are gathered in Table 4; it can be seen that a more negative E_{corr} value is obtained for bare mild steel. GNP, h-BN and h-BN/GNP nano-treatments showed comparatively less negative or higher E_{corr} values than bare mild steel, indicating their better corrosion resistance. The values of I_{corr} decreased in the order mild steel > GNP > h-BN/GNP > h-BN. Furthermore, results revealed that h-BN nanoparticles played a key role in minimising the corrosion rate of mild steel [36].

Nyquist plots (Fig. 9a) exhibit a wider diameter of the capacitive loop which directly indicates the corrosion resistance of surface treatment. Two capacitive loops were observed in the EIS data, which indicates that the corrosion process consisted of two relaxation events. The electrical equivalent circuit (EEC) model was used to curve fit the EIS data to $R_s(Q_{coat}(R_{coat}(Q_{dl}R_{ct})))$ model, as shown in Fig. 9c. R_s, R_{coat}, R_{ct}, Q_{coat}, Q_{dl} represent the solution resistance, coating resistance, charge transfer resistance, coating capacitance and double layer capacitance, respectively. A constant phase element was used instead of the capacitor to model the behaviour for the double layer.

Corrosion parameters obtained using the EEC model for all the samples are provided in Table S2. Value of Polarization resistance (R_p) where $R_p = R_{coat} + R_{ct}$ was found to be 2092.15, 2157.93, 2438.62 and 3029.95 Ω cm^2 for bare, GNP-, h-BN/GNP- and h-BN-treated samples respectively. The highest value of R_p for h-BN treated steel shows that the h-BN nanoparticles provide the highest reduction in the surface activity of the mild steel sample against a corrosive environment.

The ability of graphene to protect from corrosion is still arguable, with some evidence that long-term protection is very challenging. The nobility of graphene makes it cathodic to most metals, resulting in a fast corrosion rate once the corrosive liquid finds its way between the graphene treatment and the steel substrate. To evaluate the practical ability of the steel treated with 2D materials to resist corrosion, we have left the specimens in humid air for 6 months. To avoid any effect of the heat treatment, the bare steel sample was also heated at 300 °C. Fig. 10 shows images of the evolution of the bare steel surface and the different nano-treated surfaces after 6 months exposed to humid air. As can be seen, no sign of corrosion activity can be observed on the nano-treated surfaces after 6 months. On the other hand, clear sign of corrosion can be easily seen on the untreated steel surface. The corrosion protection using h-BN treatment is understandable since h-BN is an electrically isolating material and, therefore, not expected to form any localised cell with the substrate. The ability of the graphene treatment to protect the substrate for a long time can be referred to the good adhesion with the steel due to the partial diffusion during the heat treatment step. These results were subsequently confirmed by SEM.

The treatment with 2D materials could also protect steel from high-temperature oxidation. The SEM images of the cross-section of various specimens heated in air at 300 °C are illustrated in Fig. 11. A thick oxide

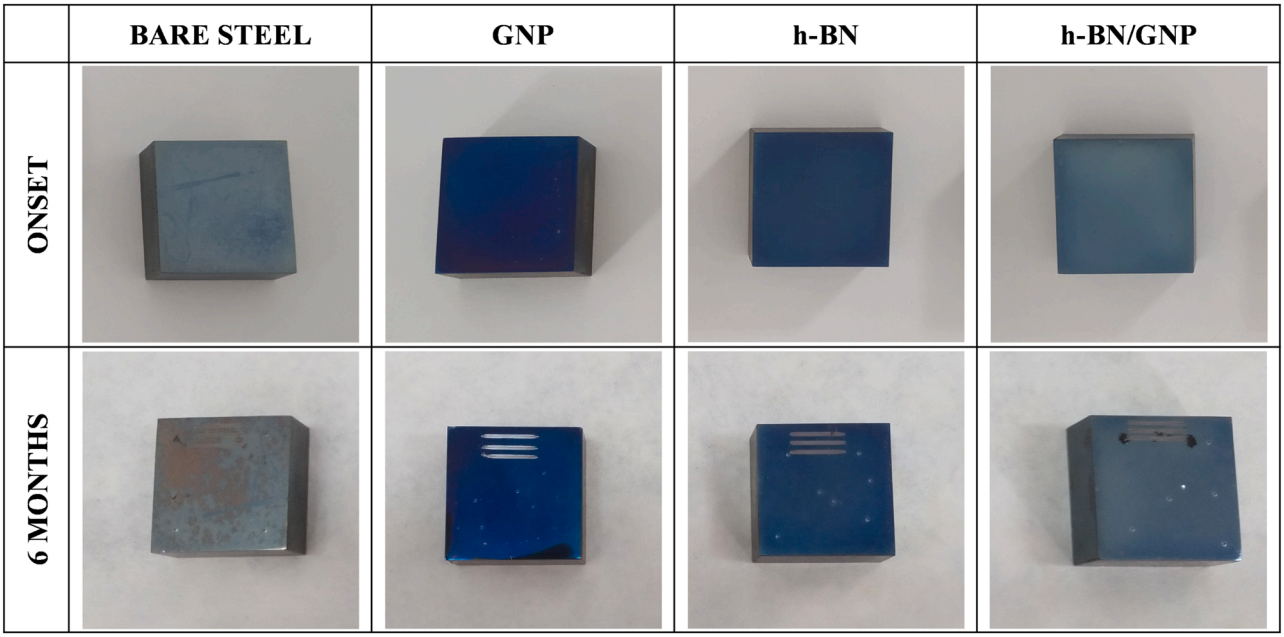

Fig. 10. Evolution of bare and treated steel substrate surfaces to ambient exposure.

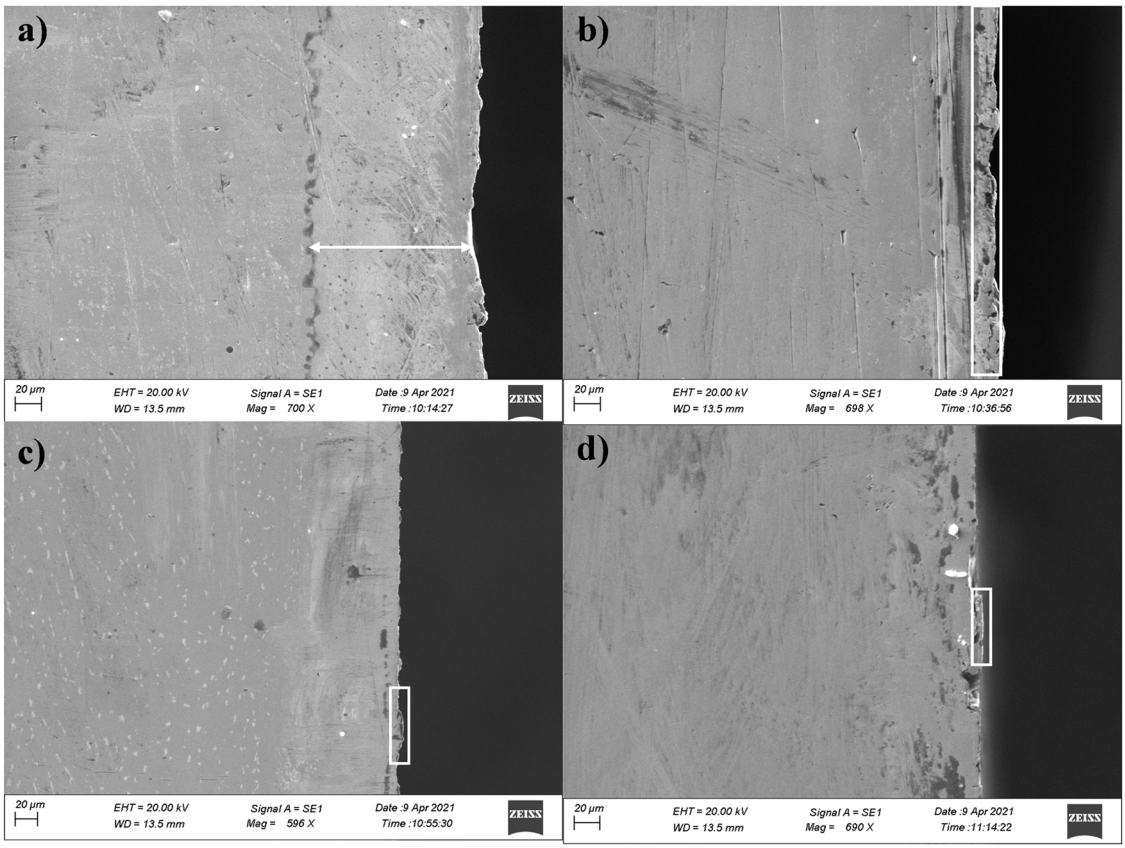

Fig. 11. Cross-sectional SEM images of (a) bare mild steel substrate and of three different nano-treated substrates: (b) GNP, (c) h-BN and (d) h-BN/GNP.

scale layer with almost 100 μm can be observed on the surface of the bare stell. An apparent gap between the oxide layer and the substrate can also be seen, suggesting weak adhesion and the possibility of peeling off. Not such a layer can be observed in any of the samples treated with GNP, h-BN, or GNP/h-BN can confirm the chemical stability of the treated steel at high temperature. The 10–20 μm layer of GNP on the steel sample can still be detected after heating (Fig. 11b), suggesting the thermal stability of the graphene coating. Especially for the h-BN treatment (Fig. 11c), the diffusion of the boron nitride (white dots) has occurred through the steel and worked as a barrier for any further oxygen diffusion or reaction with the substrate. No defects or cracks were observed at the interfaces of the nano-treated surfaces, providing evidence of good adhesion between the steel substrate and coating.

4. Conclusions

This work successfully developed nano-treated surfaces by spraying GNP and/or h-BN on mild steel surfaces followed by a gentle heat treatment at 300 °C for 4 h. Several spectroscopic analyses confirmed the uniform distribution of the 2D materials on the surface and their diffusion to the sub-micron level. Unlike traditional steel nitriding, carbonising or coating, the nano-treated surface could improve several surface properties simultaneously. First, the surface nano-treatment showed excellent wear resistance characteristics. These nano-treated surfaces revealed a wear area decrease of almost 31%, 28% and 44% for GNP, h-BN and h-BN/ GNP, respectively, compared to bare mild steel. Among all, the hybrid-treated surface revealed a maximum reduction of up to 55% in the specific wear rate in dry conditions compared to bare steel. Second, the anti-corrosion performance of mild steel substrate was successfully reduced by up to 41% for the h-BN treatment. Thirdly, the surfaces treated with h-BN showed extraordinary resistance to high-temperature oxidation. Finally, the surface hardness of the coated samples showed improvements when compared with bare metals after being heat-treated for 4 h at 300 °C. The synergic enactment of most surface properties suggested the surface treatment of steel with 2D materials could open the door for more applications of mild steel in the near future.

Statement originality

There is no conflict of interest exists in the submission of this manuscript. I would like to declare on behalf of my co-authors that the work described was original research that has not been published previously, and not under consideration for publication elsewhere, in whole or in part.

Declaration of Competing Interest

The authors declare that they have no known competing financial interests or personal relationships that could have appeared to influence the work reported in this paper.

Data Availability

Data will be made available on request.

Acknowledgments

This research is supported by projects PID2020-112846RB-C22 and ED431C 2020/10 funded by MCIN/AEI/10.13039/501100011033 and "NextGenerationEU/PRTR" and through the Xunta de Galicia, respectively. Dr M.J.G.G. also acknowledges the Xunta de Galicia (Spain) for the postdoctoral fellowship (reference ED481B-2019-015) at Bournemouth University (UK). Prof. ARK acknowledges the Fundamental

Research Funds for the Central Universities (N2025001).

Appendix A. Supporting information

Supplementary data associated with this article can be found in the online version at doi:10.1016/j.triboint.2023.108264.

References

[1] Holmberg K, Erdemir A. The impact of tribology on energy use and CO_2 emission globally and in combustion engine and electric cars. Tribol Int 2019;135:389–96. https://doi.org/10.1016/j.triboint.2019.03.024.

[2] Berman D, Erdemir A, Sumant AV. Few layer graphene to reduce wear and friction on sliding steel surfaces. Carbon 2013;54:454–9. https://doi.org/10.1016/j.carbon.2012.11.061.

[3] Davis J.R. Surface Hardening of Steels: Understanding the Basics 2002.

[4] Abbasi K, Alam S, Khan MI. An experimental study on the effect of MIG welding parameters on the Weld-Bead shape characteristics. Eng Sci Tehnol Int J 2012;2:599–602.

[5] Cui G, Bi Z, Zhang R, Liu J, Yu X, Li Z. A comprehensive review on graphene-based anti-corrosive coatings. Chem Eng J 2019;373:104–21. https://doi.org/10.1016/j.cej.2019.05.034.

[6] Kumar CMP, Chandrashekarappa MPG, Kulkarni RM, Pimenov DY, Giasin K. The effect of Zn and Zn–WO_3 composites nano-coatings deposition on hardness and corrosion resistance in steel substrate. Materials 2021;14:2253. https://doi.org/10.3390/ma14092253.

[7] Singh Raman RK, Tiwari A. Graphene: the thinnest known coating for corrosion protection. JOM 2014;66:637–42. https://doi.org/10.1007/s11837-014-0921-3.

[8] Arjmand S, Khayati GR, Akbari GH. Al/Ti5Si_3-Al_3Ti composite prepared via in-situ surface coating of Ti using tungsten inert gas welding. J Alloy Compd 2019;808:151739. https://doi.org/10.1016/j.jallcom.2019.151739.

[9] Ma N-n Chen J, Huang Z-r LiY-j, Liu M, Liu X-j, et al. Fabrication of amorphous silica coating on graphite substrate by laser cladding. Ceram Int 2020;46:10829–34. https://doi.org/10.1016/j.ceramint.2020.01.094.

[10] Yan H, Zhang P, Gao Q, Qin Y, Li R. Laser cladding Ni-based alloy/nano-Ni encapsulated h-BN self-lubricating composite coatings. Surf Coat Technol 2017;332:422–7. https://doi.org/10.1016/j.surfcoat.2017.06.079.

[11] Riyadi TWB, Zhang T, Marchant D, Zhu X. Synthesis and fabrication of NiAl coatings with Ti underlayer using induction heating. Surf Coat Technol 2014;258:154–9. https://doi.org/10.1016/j.surfcoat.2014.09.037.

[12] Song B, Murray JW, Wellman RG, Pala Z, Hussain T. Dry sliding wear behaviour of HVOF thermal sprayed WC-Co-Cr and WC-Cr_xC_y-Ni coatings. Wear 2020;442–443:203114. https://doi.org/10.1016/j.wear.2019.203114.

[13] Girotto C, Rand BP, Genoe J, Heremans P. Exploring spray coating as a deposition technique for the fabrication of solution-processed solar cells. Sol Energy Mater Sol Cells 2009;93:454–8. https://doi.org/10.1016/j.solmat.2008.11.052.

[14] Verma MY, Dhillon KS. Improvement in the wear resistance and mechanical properties of carburized mild steel by varying carburization temperature and constant tempering temperature. Int J Innov Sci Res 2015;15:379–88.

[15] Candelária A, Pinedo C. Influence of the heat treatment on the corrosion resistance of the martensitic stainless steel type AISI 420. J Mater Sci Lett 2003;22:1151–3. https://doi.org/10.1023/A:1025179128333.

[16] Zhong C, Liu F, Wu Y, Le J, Liu L, He M, et al. Protective diffusion coatings on magnesium alloys: a review of recent developments. J Alloy Compd 2012;520:11–21. https://doi.org/10.1016/j.jallcom.2011.12.124.

[17] Yang X, Zhang R, Pu J, He Z, Xiong L. 2D graphene and h-BN layers application in protective coatings. Corros Rev 2021;39:93–107. https://doi.org/10.1515/corrrev-2020-0080.

[18] Abdelkader AM, Kinloch IA, Dryfe RAW. Continuous electrochemical exfoliation of micrometer-sized graphene using synergistic ion intercalations and organic solvents. ACS Appl Mater Interfaces 2014;6:1632–9. https://doi.org/10.1021/am404497n.

[19] Abdelkader AM, Kinloch IA. Mechanochemical exfoliation of 2D crystals in deep eutectic solvents. ACS Sustain Chem Eng 2016;4:4465–72. https://doi.org/10.1021/acssuschemeng.6b01195.

[20] Metals4U. Ltd. ⟨https://www.metals4u.co.uk/blog/en3b-bright-mild-steel⟩ 2021.

[21] Guimarey MJG, Abdelkader AM, Comuñas MJP, Alvarez-Lorenzo C, Thomas B, Fernández J, et al. Comparison between thermophysical and tribological properties of two engine lubricant additives: electrochemically exfoliated graphene and molybdenum disulfide nanoplatelets. Nanotechnology 2020;32:025701. https://doi.org/10.1088/1361-6528/abb7b1.

[22] Ling J, Miao X, Sun Y, Feng Y, Zhang L, Sun Z, et al. Vibrational imaging and quantification of two-dimensional hexagonal boron nitride with stimulated Raman scattering. ACS Nano 2019;13:14033–40. https://doi.org/10.1021/acsnano.9b06337.

[23] Malard LM, Pimenta MA, Dresselhaus G, Dresselhaus MS. Raman spectroscopy in graphene. Phys Rep 2009;473:51–87. https://doi.org/10.1016/j.physrep.2009.02.003.

[24] Brumovský M, Oborná J, Micić V, Malina O, Kašlík J, Tunega D, et al. Iron nitride nanoparticles for enhanced reductive dechlorination of trichloroethylene. Environ Sci Technol 2022;56:4425–36. https://doi.org/10.1021/acs.est.1c08282.

[25] Biesinger MC, Payne BP, Grosvenor AP, Lau LWM, Gerson AR, Smart RSC. Resolving surface chemical states in XPS analysis of first row transition metals, oxides and hydroxides: Cr, Mn, Fe, Co and Ni. Appl Surf Sci 2011;257:2717–30. https://doi.org/10.1016/j.apsusc.2010.10.051.

[26] Perfetti G, Alphazan T, van Hee P, Wildeboer WJ, Meesters GMH. Relation between surface roughness of free films and process parameters in spray coating. Eur J Pharm Sci 2011;42:262–72. https://doi.org/10.1016/j.ejps.2010.12.001.

[27] Restuccia P, Righi MC. Tribochemistry of graphene on iron and its possible role in lubrication of steel. Carbon 2016;106:118–24. https://doi.org/10.1016/j.carbon.2016.05.025.

[28] Chan JX, Wong JF, Petrů M, Hassan A, Nirmal U, Othman N, et al. Effect of nanofillers on tribological properties of polymer nanocomposites: a review on recent development. Polymers 2021;13:2867. https://doi.org/10.3390/polym13172867.

[29] Shen Y, Lei W, Tang W, Ouyang T, Liang L, Tian ZQ, et al. Synergistic friction-reduction and wear-resistance mechanism of 3D graphene and SiO_2 nanoblend at harsh friction interface. Wear 2022;488–489:204175. https://doi.org/10.1016/j.wear.2021.204175.

[30] Schmitz TL, Action JE, Burris DL, Ziegert JC, Sawyer WG. Wear-rate uncertainty analysis. J Tribol 2004;126:802–8. https://doi.org/10.1115/1.1792675.

[31] Bloch HP, Geitner FK. Chapter 10 - Protecting machinery parts against the loss of surface. In: Bloch HP, Geitner FK, editors. Machinery Component Maintenance and Repair (Fourth Edition). Gulf Professional Publishing; 2019. p. 551–633.

[32] Gheisari R, Bashandeh K, Polycarpou AA. Effect of surface polishing on the tribological performance of hard coatings under lubricated three-body abrasive conditions. Surf Topogr 2019;7:045001. https://doi.org/10.1088/2051-672X/ab40ff.

[33] Liñeira del Río JM, López ER, González Gómez M, Yáñez Vilar S, Piñeiro Y, Rivas J, et al. Tribological behavior of nanolubricants based on coated magnetic nanoparticles and trimethylolpropane trioleate base oil. Nanomaterials 2020;10:683. https://doi.org/10.3390/nano10040683.

[34] Geick R, Perry CH, Rupprecht G. Normal modes in hexagonal boron nitride. Phys Rev 1966;146:543–7. https://doi.org/10.1103/PhysRev.146.543.

[35] Dovbeshko G, Cherepanov V, Boiko V, Perederiy A, Olenchuk M, Negriyko A, et al. Raman modes and mapping of graphene nanoparticles on Si and photonic crystal substrates. Opt Mater X 2022;15:100163. https://doi.org/10.1016/j.omx.2022.100163.

[36] Madhusudhana AM, Mohana KNS, Hegde MB, Nayak SR, Rajitha K, Swamy NK. Functionalized graphene oxide-epoxy phenolic novolac nanocomposite: an efficient anticorrosion coating on mild steel in saline medium. Adv Compos Hybrid Mater 2020;3:141–55. https://doi.org/10.1007/s42114-020-00142-8.